

AN ANALYSIS OF THE EFFECTS OF HELIUM ON FAST FRACTURE AND EMBRITTLEMENT OF $\approx 8\text{Cr}$ TEMPERED MARTENSITIC STEELS—G. R. Odette, T. Yamamoto, and H. Kishimoto (University of California, Santa Barbara)

OBJECTIVE

The objective of this research is to assess the effect of helium on fast fracture and irradiation embrittlement of $\approx 8\text{Cr}$ martensitic steels.

SUMMARY

We have assembled the available paired datasets on irradiation-induced increases in yield stress (σ_y) and transition temperature shifts (ΔT), in order to assess the potential role of high levels of helium on irradiation embrittlement of $\approx 8\text{Cr}$ martensitic steels. Both ΔT versus σ_y scatter plots and variations in the hardening-shift coefficient, $C = \Delta T / \sigma_y$, are used to evaluate potential non-hardening helium embrittlement (NHHE) contributions to ΔT . The available data is limited, scattered, and potentially confounded. However, collectively the database suggests that there is a minimal NHHE up to a few hundred appm. However, a NHHE contribution appears to emerge at higher helium concentrations, estimated to be more than 400 to 600 appm. The NHHE is accompanied by a transition from transgranular cleavage (TGC) to intergranular fracture (IGF). IGF generally occurs only at high σ_y . Synergistic combinations of large σ_y and severe NHHE could lead to very large ΔT in first wall and blanket structures at fusion spectrum dose levels above 50 to 75 dpa. Future research will focus on continued collection and analysis of data, participation in new experiments to better address NHHE and developing detailed micromechanical models of helium effects.

PROGRESS AND STATUS

Introduction

Two of the most important issues facing the development of normalized and tempered $\approx 8\text{Cr}$ normalized and tempered martensitic steels for fusion applications are the effects of high levels of transmutation product helium under conditions of simultaneous displacement damage production and irradiation embrittlement. Indeed, it is largely concerns about helium that have motivated the need for the International Fusion Materials Irradiation Facility. Because of the high sink density that act as traps, martensitic steels are generally believed to be relatively immune to helium effects [1,2,3]. However, at high helium levels, a significant population of bubbles forms, with number densities, sizes and spatial distributions that depend on the irradiation temperature and the alloy microstructure. The amount and distribution of helium on grain boundaries is particularly significant [4].

A key manifestation of irradiation embrittlement is an increase in transition temperature (ΔT) for fast fracture, typically measured in sub-sized Charpy V-notch type impact tests. Much attention has been directed at the effect of helium on low temperature fast fracture and embrittlement, and this issue remains a matter of significant uncertainty. One school of thought has asserted that helium plays a dominant role in embrittlement, in some cases even apparently showing a linear correlation between helium concentration and ΔT [5-14]. A contrary view attributes a dominant role to irradiation hardening induced embrittlement, where the hardening is primarily associated with displacement damage. Thus, at least up to some concentration, helium only plays a secondary role [15,16], primarily through its effect on hardening. The sensitivity of hardening to helium generally appears to be modest below very high levels. However, to date it has not been possible to obtain reliable experimental assessment of helium effects on fast fracture in candidate materials at damage rates, doses and temperatures relevant to the first wall and blanket environment. Thus there has been no clear experimental resolution of this issue.

We begin by proposing a framework to better assess the issue of helium effects on fast fracture based on existing data. It is noted that this framework has been used to design a series of experiments that are being conducted as part of the US-Japan collaborative irradiation program in the High Flux Isotope Reactor (HFIR). The framework can be described as follows:

- 1) "Brittle" fracture occurs in bcc alloys when the elevated normal stress ($\sigma_n = M\sigma_y$) in front of a notch or crack tip exceeds a critical local fracture stress for transgranular cleavage (σ_c^*) or intergranular (σ_{ig}^*) fracture over a critical microstructural volume of material (V^*), or $\sigma_n(V^*) \geq \sigma_c^*$. Here σ_y is the yield stress and M is a constraint factor that varies between about 2 to 4 depending on the notch/crack geometry and the alloy strain-hardening rate [16-18].
- 2) At low irradiation temperatures ($< \approx 375\text{-}400^\circ\text{C}$), and in the absence of high levels of helium, the ΔT is due to irradiation hardening and can be correlated with changes in yield stress ($\Delta\sigma_y$), as $\Delta T = C\Delta\sigma_y$ [15-19]. The value of the hardening-embrittlement coefficient C depends on both $\Delta\sigma_y$ and the elastic cleavage transition temperature and upper shelf energy of a particular unirradiated alloy [17].
- 3) At high irradiation temperatures ($> \approx 425^\circ\text{C}$) there is typically either little or no hardening, or some degree of softening, with $\Delta\sigma_y \leq 0$ [20]. However, positive ΔT may occur in this temperature regime as the result of reductions in σ_c^* due to irradiation enhanced thermal aging processes [16,19]. Such non-hardening embrittlement (NHE) processes include precipitation or coarsening of brittle phases, grain boundary segregation of solutes, such as phosphorous, and instabilities in the tempered martensitic substructure [9,16,19-21]. In 8Cr martensitic steels containing significant quantities of tungsten, a primary non-hardening embrittlement mechanism is precipitation of brittle Laves phases on prior austenitic grain boundaries (PAGs). Purely thermal NHE occurs at $\approx 500^\circ\text{C}$ and above; but it appears that radiation enhanced diffusion decreases to lower leg of the time-temperature NHE C-curve to about 400°C or less [16,19]. This is a concern, since combinations of $\Delta\sigma_y$ and NHE may give rise to very large ΔT . Significant NHE is signaled by large, or alternatively, negative (when $\Delta T > 0$ and $\Delta\sigma_y < 0$) values of C and, often, a transition from transgranular cleavage (TGC) to intergranular fracture (IGF).
- 4) The accumulation of helium and hydrogen on PAGs may also lead to NHE. We will focus on the potential effect of large amounts of helium and NHHE, but in some cases this cannot be distinguished from a corresponding high concentration of hydrogen. The distribution of helium on the grain boundaries is critical. For example, a coarse distribution of large bubbles would be expected to have little effect on ΔT , while a monolayer-type film of boundary would likely be most damaging [16].
- 5) As noted above, NHE and NHHE are generally associated with a transition from a TGC to IGF local fracture mode. While oversimplified, a conceptual model of the competing effects TGC versus IGF is very useful. The model posits that the TGC continues to be the fracture path of least resistance as long as it has a lower critical stress than that for IGF. Thus, gradual weakening of the PAGs by helium (and/or other mechanisms) would not be reflected in IGF until σ_{ig}^* falls below σ_c^* , where ΔT depends synergistically on both $\sigma_{ig}^* - \sigma_c^*$ (< 0) and $\Delta\sigma_y$. Of course in reality the transition would not be abrupt and the conceptual model is oversimplified.
- 6) High levels of helium may also contribute an increment of hardening beyond that due to displacement damage alone. However, the incremental hardening appears to be modest up to fairly high concentration [1,19,22-24], at least at lower irradiation temperature

- 7) A number of experimental studies have used nickel doping to produce high concentrations of helium by two-stage $^{58}\text{Ni}(n, \alpha) \rightarrow ^{59}\text{Ni}(n, \alpha)$ reactions. It is well established that nickel additions result in additional hardening at lower irradiation temperatures [25-28]. This may be due to enhancement of hardening from defect clusters as well as fine scale nickel enriched precipitates. More generally, nickel additions change the transformation temperatures and kinetics in quenched and tempered steels, hence, modifying the overall microstructure. Thus increases in ΔT associated with nickel doping may or may not be due to helium.
- 8) Doping with boron isotopes (natural boron is 0.2 ^{10}B and ≈ 0.8 ^{11}B) can also be used to produce large quantities of helium from the $^{10}\text{B}(n, \alpha)^6\text{Li}$ thermal neutron reaction. However, the solubility of boron in steels is extremely low, and boron doping is also confounded by: a) the non-uniform distributions, which tends to segregate boron at PAGs and other interfaces and/or to form boride precipitate phases; b) boron's general effects on the microstructure and properties of quenched and tempered alloys; c) boron's role in strengthening grain boundaries; d) the production of equal amounts of transmutant lithium and helium while eliminating boron; d) very rapid transmutation and burn-out of boron at relatively low dpa; and, e) at low doses, excess dpa due to recoils from the n, α reactions.
- 9) The effects of such confounding factors can be partially mitigated by careful experimental designs. For example, comparisons of ΔT in paired alloys doped with either ^{58}Ni or ^{60}Ni (alternatively ^{10}B or ^{11}B) can help isolate the independent effect of helium.

Since the effects of fusion relevant helium levels on hardening appear to be modest, the major issue is the potential role of helium in NHHE. The framework outlined above has been incorporated in recent experiments. For example, a single variable experiment is being carried out to compare the ΔT , $\Delta\sigma_y$ and C for martensitic alloys doped with ^{58}Ni and ^{60}Ni isotopes as well as natural Ni; and another experiment is planned that will use alloys doped with ^{10}B and ^{11}B isotopes. However, these principles are generally not reflected in past studies. Indeed, most previous experiments did not even include tensile specimens to provide $\Delta\sigma_y$ data as a complement to the ΔT measurements from sub-sized Charpy tests; and even the simple expedient of microhardness measurements to estimate irradiation hardening was rarely exploited. Further, there have been relatively few fractographic studies to characterize the local fracture mode, and any transitions from TGC to IGF in irradiated alloys as a function of helium content.

Nevertheless, it is still possible to analyze existing data to try to detect, and even quantitatively estimate, the potential NHHE by examining the relation between ΔT and $\Delta\sigma_y$ and/or $C = \Delta T / \Delta\sigma_y$. Specifically, C accounts for the primary hardening induced embrittlement and, to first order, resolves many (not all) of the confounding factors. Large increases in C with increasing helium signal a NHHE contribution and vice versa. Of course, even if C appears to increase with helium, NHHE is not assured due to the confounding factors. Further, uncertainties in C must also be considered. Even relatively optimistic estimates of uncertainties of only $\pm 10^\circ\text{C}$ in ΔT and ± 20 MPa in $\Delta\sigma_y$ result mean uncertainties in C of $\approx \pm 10 / \Delta T$ for an actual $C = 0.4^\circ\text{C}/\text{MPa}$. Thus a relatively large scatter in C values should be anticipated, particularly at small ΔT , and it is always useful to examine ΔT versus $\Delta\sigma_y$ scatter plots as well as the trends in C. Of course there are other indicators of NHHE. The most significant is the transition from TGC to IGF above some critical level of helium [1,24,29].

Analysis of the Existing ΔT - $\Delta\sigma_y$ Database and the Effects of He

We have assembled available information in cases in which it was possible to obtain reasonably good estimates of pairs of $\Delta\sigma_y$ and ΔT data. The most relevant ΔT data are based on sub-sized Charpy tests [7,8,30-38]. Unfortunately, due to the failure to include tensile specimens in many experiments, such data is limited. Other issues are that the tensile data is confined to tests at the elevated irradiation temperature

(or greater), where the σ_y are smaller than at lower temperatures pertinent to the ΔT measured in sub-sized Charpy tests [20]. Thus when possible, we use σ_y from room temperature tests. In addition to separate tensile (or hardness) tests it is possible to extract dynamic yield stress (σ_{yd}) values from the load-time data provided by instrumented sub-sized Charpy V-notch impact tests. Unfortunately, σ_{yd} information is seldom reported. An exception is the case of a large embrittlement database developed in Germany and summarized in a recent report and papers [7,8,30]. The alloys in these studies contained various amounts of natural B, thus had different levels of helium following mixed spectrum irradiations. Hence, we were able to obtain paired data σ_{yd} - ΔT .

There are also pertinent data from for spallation proton irradiations based on so-called small punch (SP) tests that can be used to estimate both irradiation hardening and transition temperature shifts [15,29,39]. However the SP technique is not true fracture tests per se. An effective yield stress (σ_{yp}) and corresponding irradiation hardening ($\Delta\sigma_{yp}$) are evaluated based on the nonlinearities in punch load-displacement curves. An effective transition temperature (T_{sp}) and irradiation induced shifts (ΔT_{sp}) are determined by plotting the integrated load-displacement energy at fracture, measured at the point of a large load drop, as a function of the test temperature. Since SP tests are inherently involve static, low constraint conditions, with small values of M (or ratios of the maximum principal stress relative to the σ_y) the brittle (TGC or IGF) to ductile transition, if any, occurs at temperatures that are much lower than for standard, and even sub-sized, Charpy impact tests; and the corresponding shifts in ΔT_{sp} , due to embrittlement, are also much lower than ΔT . An empirical adjustment of $\Delta T \approx 2.5\Delta T_{sp}$ is used in this report to evaluate ΔT and C [15,29,39-41] Finally, while highly unusual in steels, brittle fracture may also occur in tensile tests with lower bound values of $M = 1$. As noted above this implies a very low value of the critical brittle fracture stress. However, even in a tensile test M is greater than 1 in the necked region beyond the uniform strain limit. The maximum M increases with necking and can be related to the reduction in area at fracture and the corresponding tri-axial stresses in the necked region.

Figure 1a and b summarizes the very limited available Charpy-tensile test ΔT versus σ_y data with helium variations in nominally similar alloys with and without nickel or boron doping for irradiations at ≈ 300 and 400°C respectively [31-38]. Helium content shown in parenthesis is common for both of Charpy and tensile specimens except for some cases where data for a common condition are not available; in these cases, both values of (Charpy/tensile) specimens are shown. The dashed lines indicate the scatter in the general database for ΔT versus σ_y [19]. Two data sets are for a 9CrMo alloy both undoped and doped with 2%Ni irradiated at 300 and 400°C . The nickel doping results in increases from ≈ 14 to 234 and 33 to 369 appm He in these cases, respectively. Both the doped and undoped alloys fall on virtually the same ΔT versus σ_y line with $C = 0.40$ $^\circ\text{C}/\text{MPa}$ at 300°C and $C = 0.82 \pm 0.02$ $^\circ\text{C}/\text{MPa}$ at 400°C . Thus while the nickel addition increases the σ_y in these cases, there is no independent NHHE effect of either nickel or helium indicated by this data set. The corresponding ΔT for a 9Cr2W alloy doped with 2% nickel irradiated at $\approx 300^\circ\text{C}$ with ≈ 115 appm He falls slightly above the ΔT versus σ_y line for the corresponding undoped steel with ≈ 5 appm helium, with C of 0.44 and 0.32 $^\circ\text{C}/\text{MPa}$ respectively. However, both are well within the overall ΔT versus σ_y and C scatter band. A generally similar result is found for natural B doped F82H and JLF1 steels irradiated at 300°C , with ≈ 23 -40 appm He, compared to undoped alloys with ≈ 3 appm He. These results may suggest a slightly stronger effect of boron compared to nickel doping, with values of ≈ 0.53 and 0.75 (high helium) versus 0.43 and 0.58 (low helium).

Figure 1a and b also show ΔT versus σ_y for 12Cr1Mo Ni-doped and undoped alloys also indicating no effect of helium and the data all fall within the normal scatter bands [36-38]. However, a recent review paper included 300°C data on F82H doped with various isotopes of B showed a systematic increase of C with increasing helium up to 340 appm [42,43]. Thus these results may also suggest a stronger effect of boron compared to nickel doping, perhaps due to B segregation to PAGs. Overall, however, the very the limited nickel and boron doping data show little effect of helium on C up to concentrations ≈ 300 appm.

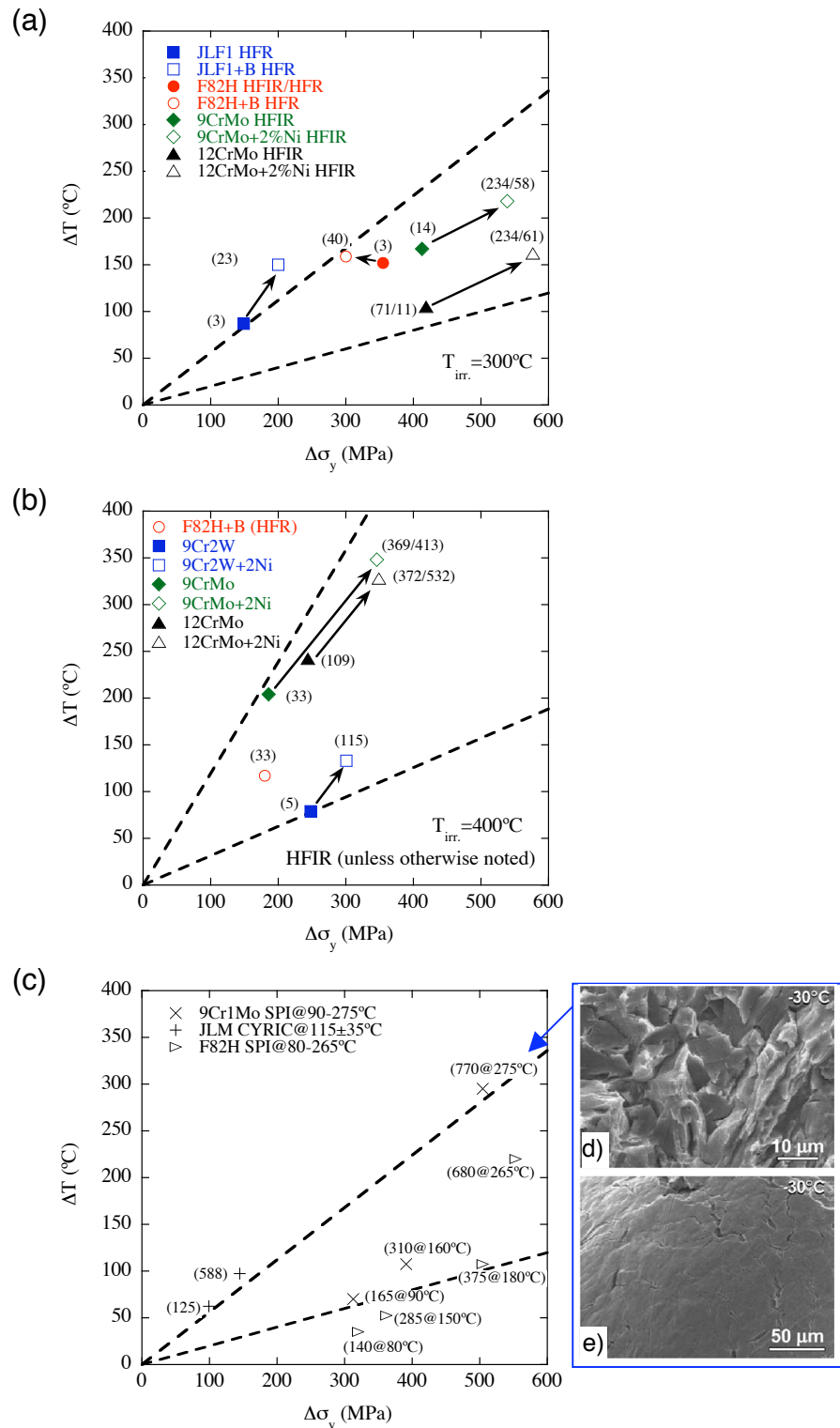


Figure 1. (a) Charpy ΔT versus tensile σ_y data with helium variations in nominally similar steels with and without B- or Ni-doping irradiated at 300 °C and (b) at 400 °C. (c) SP ΔT_p versus σ_{yp} data with helium variations after SPI along with ΔT_p versus σ_{ym} data with helium variations. (d) Fracture surface and (e) bottom surface of punch-tested specimen with 770 appm He/9.4 dpa showing the occurrence of IGF from reference 29. [11,19,29,31-38].

Dai and co-workers have reported a nearly linear correlation between the helium level and ΔT for spallation proton irradiations (SPI) of 9Cr1Mo T91 and F82H steels at nominal temperatures between ≈ 90 to 275 °C from ≈ 2.5 to 9.4 dpa producing ≈ 140 to 770 appm He [29,39]. Note the temperatures, He levels and dpa generally increase in tandem. Figure 1c shows plot of this SP ΔT_p versus $\Delta\sigma_{yp}$ data. The helium levels and nominal irradiation temperatures are shown in the parenthesis near each data point. At the intermediate helium levels, the data fall in the lower region of the overall ΔT versus $\Delta\sigma_y$ scatter band for this irradiation temperature range shown by the dashed lines. Jia and Dai also noted the fact that these data fall in the general scatter band of ΔT versus dpa for fission irradiations [39]. However, there is a distinct break in the ΔT_p versus $\Delta\sigma_{yp}$ trend for the data points at 680 appm He in F82H and 770 appm He in T91. Although the corresponding C values are neither particularly high, nor anomalous, the onset of significant amounts of IGF are observed in these cases, suggesting the emergence of a NHE contribution at very high helium levels. Note, IGF is readily observed both on the fracture surfaces and as a network of grain boundary cracks on the bottom surface of the SP disc as shown in the micrographs taken from reference 29. (Figures 3d and 3e.)

Of course, the SPI results based on SP tests do not represent single variable experiments, and interpretations of this should be viewed with considerable caution. For example, high levels of hydrogen and other transmutation products may also play a role in the larger C observed at the highest spallation proton dose, confounding unambiguous conclusions about the effects of helium acting alone. Figure 1c also shows ΔT_p versus $\Delta\sigma_{ym}$ data for 36 MeV α -ion irradiations to 100 and 600 appm He at 115 ± 35 °C based on SP assessments of ΔT_{sp} and hardening evaluated using Vickers microhardness tests ($\Delta\sigma_{ym}$) [15]. In this case, the ΔT_p versus $\Delta\sigma_{ym}$ data fell near the top of the general scatter-band, but there was essentially no effect of helium on the ΔT_p versus $\Delta\sigma_{ym}$ relation.

Another useful source of paired ΔT - $\Delta\sigma_{yd}$ data has been developed by Schneider and co-workers on a variety of steels that 'happen to have' different natural boron contents [7,8,30]. The Schneider database includes mixed spectrum neutron irradiations from 0.2 to 2.4 dpa at temperatures between 250 and 450°C that produce up to ≈ 120 appm helium. Based on empirical plots of ΔT versus helium for subsets of this database various authors [5,6] have also suggested a dominant role of helium on embrittlement. Indeed, fits to the overall database for $T < 400$ °C do result in a weak correlation that would indicate a strong effect of helium, that would, if true, result in an enormous $\Delta T \approx 1080$ °C at 1000 appm He. Note, the 450°C data indicates that ΔT decreases with increasing helium, but is excluded from this analysis, since the C are very scattered and, on average, systematically larger than those observed at lower irradiation temperatures, indicating a NHE mechanism that is not related to helium. This is consistent with other observations of increased C at higher temperatures [16], but is not pertinent to the assessment of NHHE. Even restricting the analysis to 400°C or less, the ΔT versus helium data is very scattered and the statistical significance of the apparent correlation is low, with $r^2 \approx 0.21$.

However, a much more significant shortcoming of this sort of analysis is that it neglects the large range of $\Delta\sigma_{yd}$ in the irradiated steels. This masks the combined effects of both differences dose (dpa) as well as the wide range of metallurgical variables representing the various alloys in the Schneider database. Both $\Delta\sigma_y$ and $C = \Delta T / \Delta\sigma_{yd}$, hence the corresponding ΔT , depend on these variables, in a way that is largely independent of either the alloy boron or helium content. Note, C itself also increases with $\Delta\sigma_y$ and depends as the alloy microstructure and unirradiated Charpy properties [14]. At lower irradiation temperatures, $\Delta\sigma_y$ is the most significant factor in controlling ΔT , thus it must be accounted *before* attempting to evaluate any potential effects of any other variables.

Notably, three of the alloys with the highest boron contents in the Schneider database also contained significant quantities of nickel (0.66 to 0.92%Ni). At 300°C, the $\Delta\sigma_{yd}$ in these nickel-bearing alloys is higher by an overall average factor of $\approx 1.6 \pm 0.25$ relative to a set of nominally similar nickel free alloys. Indeed, there is a systematic overall correlation between $\Delta\sigma_y$ and the alloy nickel content. The nicke85

sensitivity of σ_y decreases with irradiation temperature, dropping significantly between 350 and 400°C. Figure 2a shows that the σ_T versus σ_{yd} generally fall in the same scatter band as the larger overall database for $\approx 8\text{Cr}$ tempered martensitic steels as shown by the dashed lines. Figure 2b plots the corresponding $C = \sigma_T/\sigma_{yd}$ as a function of helium content. Least squares fits show an apparently significant effect of higher helium increasing σ_T only for the data for irradiations at 250°C; and in the case, the effect of helium is primarily manifested in the range below 50 appm He. The fits for the largest set of data for irradiations at 300°C show only a weak apparent effect of helium, while at higher temperatures there is a negative association between helium and C . A best fit to all the C data in the Schneider database for irradiations at $\leq 400^\circ\text{C}$ shown by the solid line, indicates a very weak, statistically insignificant, negative effect of helium. These results are not surprising, since all but one data point is below 100 appm helium. The scatter in C is consistent with expectations and the $C = 0.41 \pm 0.2 \text{ MPa}/^\circ\text{C}$, shown by the horizontal dashed lines, are very consistent with the corresponding values for the larger overall $\approx 8\text{Cr}$ martensitic steels database [16].

Figure 2c re-plots the C versus helium Schneider database along with paired lower-higher helium C values for $\approx 8\text{Cr}$ alloys from Figures 1a and b shown as heavy solid lines [19]. These data show a generally weak effect of helium on C . Figure 2c also shows the relation between C and helium for the SP test data from Dai and Kasada as heavy dashed lines [15,29]. At lower helium levels the C for the Dai data the C that fall near the lower bound of the scatter band, but they increase with increasing helium in this case, falling above the nominal mean value at the highest in the range of 680 to 770 appm He. Given the atypical nature of the SP test, it is also useful to examine the relative variations of C when the SP data are normalized to a more typical value of $0.4^\circ\text{C}/\text{MPa}$ at the lowest helium as shown the dotted lines. The normalized C for the SP tests exceed $1^\circ\text{C}/\text{MPa}$ at the highest helium level, consistent with a significant NHHE effect and the observation of IGF.

Another data set published by Henry and co-workers [4] at least indirectly pertinent to the issue of NHE are the results of tensile tests at 25 and 250°C following spallation proton irradiations of a 9Cr1Mo (EM10) steel in various thermo-mechanical treatment conditions at $\approx 260^\circ\text{C}$ to $\approx 9.8 \text{ dpa}$ and 750 appm He. The alloy conditions included as-tempered (AT), as-quenched (AQ) and tempered and cold-worked (CW). A strong effect of the alloy thermo-mechanical treatment and test temperature was observed in this dataset. In three cases the specimens failed after considerable deformation at reductions in area (RA) from about 44-48% that were somewhat less than the corresponding RAs of 58 to 68% in the unirradiated condition. The ductility varied with test temperature and thermo-mechanical treatment condition and increased with decreasing σ_y (given in the parenthesis) in the order: AT at 250°C (960 MPa); AT at 25°C (1150 MPa) and CW at 25°C (1220 MPa). The fracture surfaces were a mixture of ductile microvoid coalescence and cleavage with some IGF and transverse cracking. Assuming there is no strain hardening, the average fracture stress in the necked region is on the order of $\approx 2000 \text{ MPa}$ consistent with typical values of σ_c^* . Indeed, the principal tri-axial stress would be even higher in the necked region, and this may compensate for some level of strain softening. The AQ alloy tested at 25°C had the largest σ_y of 1320 MPa and lowest ductility with a RA of only 2% and $\approx 100\%$ IGF. Given the small amount of necking prior to fracture it is not unreasonable to assume that $\sigma_{ig}^* = \sigma_y \approx 1300 \text{ MPa}$, which is much lower than typical values of σ_c^* . This low value may at least in part be due to the high level of helium. This conclusion is supported by the observation that the fracture mode was $\approx 100\%$ ductile microvoid coalescence after neutron irradiations of the AQ alloy to a slightly higher strength $\sigma_y \approx 1330 \text{ MPa}$. A comparison of the fracture surfaces for the neutron and spallation proton irradiations is shown in Figure 3

Jung and co-workers [44] have reported the results of tensile tests at 25 and 250°C on EM10 and T91 after high-energy ϕ -implantation at 250°C to 0.8 dpa and 5000 appm He that result in an $\approx 0\%$ RA, $\approx 100\%$ IGF and $\sigma_y = 1079$ to 1217 MPa. The ductility was much higher and the σ_y much lower after ϕ -implantations at 550°C. The RA was much also lower for tensile tests at 550°C compared to 2586

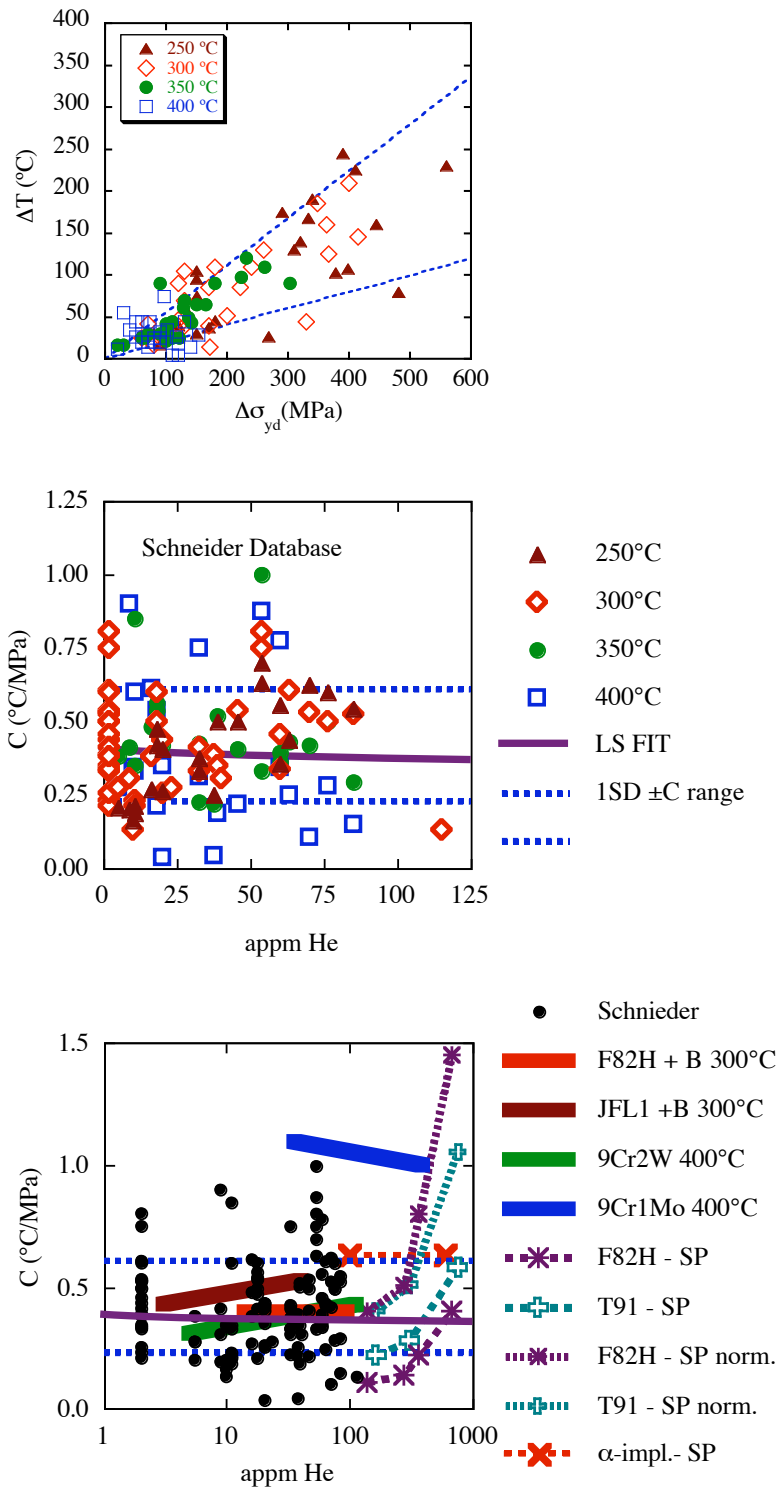


Figure 2. (a) ΔT versus $\Delta \sigma_{yd}$ from Schneider's database compared to the overall scatterband for martensitic steels irradiations at ≤ 400 . (b) $C = \Delta T / \Delta \sigma_{yd}$ for Schneider's database as a function of helium content with a least squares fit line. (c) C values from Schneider database along with paired lower-higher helium C values from Figures 1a and b shown as heavy solid lines [11,19, 30-38].

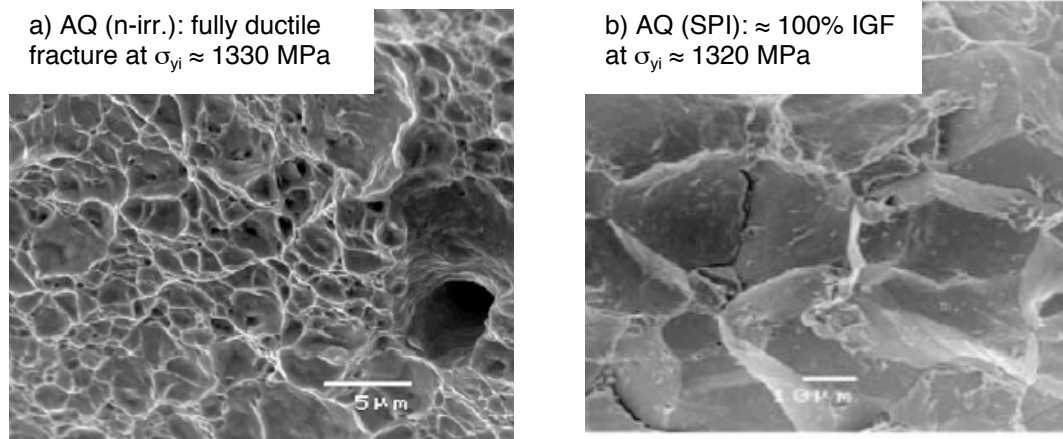


Figure 3. Tensile fracture surfaces of AQ alloy of 9CrMo steel after (a) neutron and (b) spallation proton irradiations to the similar levels of hardening at ≈ 250 °C showing ductile and IGF, respectively [from reference 4].

While no firm conclusions can be drawn from the tensile data, it is extremely significant that $\approx 100\%$ IGF is observed at normal stress levels in the range of ≈ 1100 MPa (5000 appm He) to 1300 MPa (750 appm He). Further the results suggest that in addition to helium itself, NHE and IGF also depend on both the irradiation and test temperatures. Of course the presence of cracks or notches and/or high loading rates would make materials that are so brittle in a static tensile test even more so in normal fracture tests.

Summary

We have collected and analyzed a variety of data pertinent to the issue of the effect of helium on fastfracture and irradiation embrittlement by evaluating the relation between σ_T and $\sigma_{0.2}$. The hardening-shift relation was assessed both in terms of σ_T versus $\sigma_{0.2}$ scatter plots and trends in $C = \sigma_T/\sigma_{0.2}$. Large values of C , as well as transition from TGC to IGF, at high helium concentrations were used as signatures of possible NHHE. While the data is scattered, and to some degree confounded by uncontrolled variables, the results suggest that up to concentrations several hundred appm, helium has little effect on C or σ_T . However, at higher concentrations the data is consistent with the hypothesis that accumulation of helium weakens PAG to the point where a NHHE effect emerges as signaled by higher C and IGF. This hypothesis is supported by the results of tensile tests on steels in a high strength AQ-irradiated state or implanted with very high concentrations of helium.

Future Work

Work during the next reporting period will focus on developing models of NHHE embrittlement, analysis of additional data as it becomes available and participation in the implementation of a new series of well-designed irradiations experiments in HFIR that will better address the issue of helium effects on fast fracture and embrittlement. These experiments will include pre-cracked fracture and tensile specimens that are doped with isotopes of nickel and boron that will allow evaluation the effects of up to very high concentrations of helium in alloys that are otherwise very similar. Further, we have initiated discussions with Dr. Y. Dai at PSI about establishing an active collaboration to carry out tensile, hardness and fracture tests on martensitic alloys that have been irradiated with spallation protons at low-to-intermediate temperatures up to very high $\sigma_{0.2}$ and concentrations of helium.

Aknowledgements

The authors explicitly acknowledge the extensive research that produced the data analyzed in this report and thank the researches cited in the references for their major contributions to the development of materials for fusion reactors.

References

- [1] P. Jung, C. Liu, and J. Chen, *J. Nucl. Mater.* 296 (2001) 165.
- [2] A. Kimura, R. Kasada, K. Morishita, R. Sugano, A. Hasegawa, K. Abe, T. Yamamoto, H. Matsui, N. Yoshida, B. D. Wirth, and T. D. Rubia, *J. Nucl. Mater.* 307-311 (2002) 521.
- [3] A. Hasegawa, H. Shiraishi, H. Matsui, and K. Abe, *J. Nucl. Mater.* 212-215 (1994) 720.
- [4] J. Henry, M.-H. Mathon, and P. Jung, *J. Nucl. Mater.* 318 (2003) 249.
- [5] M. Rieth, B. Dafferner, and H.-D. Rohrig, *J. Nucl. Mater.* 258-263 (1998) 1147.
- [6] R. Lindau, A. Möslang, D. Preininger, M. Rieth, and H. D. Röhrig, *J. Nucl. Mater.* 271-272 (1999) 450.
- [7] H.-C. Schneider, B. Dafferner, and J. Aktaa, *J. Nucl. Mater.* 295 (2001) 16.
- [8] H.-C. Schneider, B. Dafferner, and J. Aktaa, *J. Nucl. Mater.* 321 (2003) 135.
- [9] B. Van der Schaaf, D. S. Gelles, S. Jitsukawa, A. Kimura, R. L. Klueh, A. Möslang, and G. R. Odette, *J. Nucl. Mater.* 283-287 (2000) 52.
- [10] B. Van der Schaaf, *Harde ning and toughness from Radiation and resistance characterization of F82H and Screening Steels*, NRG Petten 20027/99.25387/P.
- [11] R. L. Klueh and D. J. Alexander, *J. Nucl. Mater.* 187 (1992) 60.
- [12] R. L. Klueh and D. J. Alexander, *J. Nucl. Mater.* 218 (1995) 151.
- [13] R. L. Klueh, D. S. Gelles, S. Jitsukawa, A. Kimura, G. R. Odette, B. van der Schaaf, and M. Victoria, *J. Nucl. Mater.* 307-311 (2002) 455.
- [14] K. Shiba, M. Suzuki, and A. Hishinuma, *J. Nucl. Mater.* 233-237 (1996) 309.
- [15] R. Kasada, T. Morimura, A. Hasegawa, and A. Kimura, *J. Nucl. Mater.* 299 (2001) 83.
- [16] G. R. Odette, T. Yamamoto, H. J. Rathbun, M. Y. He, M. L. Hribernik, and J. W. Rensman, *J. Nucl. Mater.* 323 (2003) 313.
- [17] G. R. Odette, P. M. Lombrozo, and R. A. Wullaert, *ASTM-STP 870* (1985) 841.
- [18] G. R. Odette and M. Y. He, *J. Nucl. Mater.* 283-287 (2000) 120.
- [19] T. Yamamoto, G. R. Odette, and H. Kishimoto, *Fusion Materials Semiannual Report 7/1 to 12/31/2003*, DOE/ER-313/34.
- [20] L. Schäfer, *J. Nucl. Mater.* 283-287 (2000) 707.
- [21] H. Sakasegawa, T. Hirose, A. Kohyama, Y. Katoh, T. Harada, K. Asakura, and T. Kumagai, *J. Nucl. Mater.* 307-311 (2003) 490.
- [22] L. K. Mansur, *J. Nucl. Mater.* 318 (2003) 14.
- [23] K. Farrell and T. S. Byun, *J. Nucl. Mater.* 296 (2001) 129.
- [24] J. Henry, X. Averty, Y. Dai, P. Lamagnère, J. P. Pizzanelli, J. J. Espinas, and P. Wident, *J. Nucl. Mater.* 318 (2003) 215.
- [25] R. Kasada, A. Kimura, H. Matsui, and M. Narui, *J. Nucl. Mater.* 258-263 (1998) 1199.
- [26] G. R. Odette and G. E. Lucas, *Rad. Eff. and Deff. in Solids* 144 (1998) 189.
- [27] G. R. Odette, G. E. Lucas, D. Klingensmith, B. D. Wirth, and D. Gragg, *NUREG/CR-6778* (2002).
- [28] G. R. Odette, T. Yamamoto, and D. Klingensmith, *Phil. Mag.* (2004) (in print).
- [29] Y. Dai, X. J. Jia, and K. Farrell, *J. Nucl. Mater.* 318 (2003) 192.
- [30] H.-C. Schneider, B. Dafferner, H. Ries, and O. Romer, *Irradiation Programme MANITU: Results of impact tests with the irradiated materials (2.4 dpa)*, FZKA-6605, Forschungszentrum Karlsruhe (2001).
- [31] R. L. Klueh, M. Sokolov, K. Shiba, Y. Miwa, and J. P. Robertson, *J. Nucl. Mater.* 283-287 (2000) 478.
- [32] E. V. van Osch, M. G. Horsten, G. E. Lucas, and G. R. Odette, *Effects of Radiation on Materials: 19th International Symposium*, ASTM STP 1366 (2001) 612.
- [33] E. V. van Osch, J. B. M. Bakker, R. den Boef, and J. Rensman, *NRG Petten 20023/99.26974/P*.

- [34] J. Rensman, J. van Hoepena, J. B. M. Bakker, R. den Boef, F. P. van den Broek, and E. D. L. van Essen, *J. Nucl. Mater.* 307-311 (2002) 245.
- [35] R. L. Klueh and D. J. Alexander, *J. Nucl. Mater.* 179-181 (1991) 733-736.
- [36] R. L. Klueh and P. J. Maziasz, *J. Nucl. Mater.* 187 (1992) 43-54.
- [37] R. L. Klueh and D. J. Alexander, *J. Nucl. Mater.* 187 (1992) 60.
- [38] R. L. Klueh and J. M. Vitek, *J. Nucl. Mater.* 150 (1987) 272.
- [39] X. Jia and Y. Dai, *J. Nucl. Mater.* 323 (2003) 360.
- [40] Y. Ruan, P. Spaetig, and M. Victoria, *J. Nucl. Mater.* 307-311 (2003) 236.
- [41] J. Kameda and X. Mao, *J. Mater. Sci.* 27 (1992) 983.
- [42] S. Jitsukawa et. al., ICFRM-12.
- [43] K. Shiba and A. Hishinuma, *J. Nucl. Mater.* 283-287 (2000) 474.
- [44] P. Jung, J. Henry, J. Chen, and J.-C. Brachet, *J. Nucl. Mater.* 318 (2003) 24